Electrostatics of Cell Membranes

Kevin Cahill
cahill@unm.edu
Biophysics Group, Department of Physics & Astronomy, University of New Mexico, Albuquerque, NM 87131

January 21, 2011

ABSTRACT The electrostatic potential due to a charge in or near the plasma membrane of a eukaryotic cell is computed and applied to the transduction of cell-penetrating peptides and to the exocytosis of neurotransmitters.

I. CELL MEMBRANES

The plasma membrane of a eucaryotic cell and the membranes of the endoplasmic reticulum, the Golgi apparatus, and other membrane-enclosed organelles are lipid bilayers about 5-nm-thick studded with proteins. Membrane proteins make up about half the mass of animal cell membranes. The lipids are mainly phospholipids, sterols, and glycolipids.

Of the four main phospholipids in membranes, three—phosphatidylethanolamine (PE), phosphatidylcholine (PC), and sphingomyelin (SM)—are neutral, and one, phosphatidylserine (PS), is negatively charged. In a living cell, PE and PS are mostly in the cytosolic layer of the plasma membrane; PC and SM are mostly in the outer layer [1, 2]; and the electrostatic potential of the cytosol is 20 to 120 mV lower than that of the extracellular environment.

The electrostatic potential due to a charge in a cell membrane is derived in Section II and in the Appendix. The electrostatic potential due to a charge in the extracellular environment but near the plasma membrane was derived in a recent paper [3] and is discussed in Section III. In Section IV, a symmetry argument is used to convert that solution to the potential of a charge in the cytosol but near the plasma membrane.

These solutions show that the plasma membrane shields the cytosol almost completely from charges in the extracellular environment. It follows, somewhat counter intuitively, that the electric field inside the lipid bilayer is greater than a naive estimate would suggest. Such more intense electric fields enhance the sensitivity of transmembrane proteins and make electroporation, discussed in Section V, more likely. These ideas are applied to the transduction of oligoarginines in Section VI and to the exocytosis of neurotransmitters in Section VII. The paper ends in Section VIII with some remarks about free energy and the brain inspired by Emonet's *qbio4* talk on how bacteria use noise to forage.

II. THE POTENTIAL DUE TO A CHARGE IN THE LIPID BILAYER

Here we derive in the continuum limit the electrostatic potential $V(\rho, \phi, z)$ in cylindrical coordinates due to a charge q on the z-axis at the point $(0, 0, h)$ in the phospholipid bilayer of a eukaryotic cell. We use coordinates in which $z = 0$ labels the middle of the lipid bilayer. If $t \approx 5$ nm is the thickness of the phospholipid bilayer, then the cytosol is the region $z < -t/2$, and the extracellular medium is the region $z > t/2$.

In electrostatic problems, Maxwell's equations reduce to Gauss's law

$$\boldsymbol{\nabla} \cdot \mathbf{D} = \rho \tag{1}$$

which relates the divergence of the electric displacement $\mathbf{D}$ to the density ρ of free charges (charges that are free to move in or out of the dielectric medium—as opposed to those that are part of the medium and bound to it by molecular forces), and the static form of Faraday's law

$$\boldsymbol{\nabla} \times \mathbf{E} = 0 \tag{2}$$

which implies that the electric field $\mathbf{E}$ is the gradient of an electrostatic potential

$$\mathbf{E} = -\boldsymbol{\nabla} V. \tag{3}$$

Across an interface with normal vector $\hat{\mathbf{n}}$ between two dielectrics, the tangential component of the electric field is continuous

$$\hat{\mathbf{n}} \times (\mathbf{E}_2 - \mathbf{E}_1) = 0 \tag{4}$$

while the normal component of the electric displacement jumps by the surface density σ of free charge

$$\hat{\mathbf{n}} \cdot (\mathbf{D}_2 - \mathbf{D}_1) = \sigma. \tag{5}$$

In a linear dielectric, the electric displacement $\boldsymbol{D}$ is proportional to the electric field $\boldsymbol{E}$

$$\boldsymbol{D} = \epsilon \, \boldsymbol{E} \tag{6}$$

and the coefficient ϵ is the permittivity of the material. The permittivity $\epsilon(m)$ of a material m differs from that of the vacuum ϵ_0 by the electric susceptibility χ and by the relative permittivity ϵ_m

$$\epsilon(m) = \epsilon_0 + \chi = \epsilon_m \, \epsilon_0. \tag{7}$$

The relative permittivity ϵ_m often is denoted K_m.

The lipid bilayer is taken to be flat and of a thickness $t \approx 5$ nm. The relative permittivity of the lipid bilayer is

$\epsilon_\ell \approx 2$, that of the extra-cellular environment is $\epsilon_w \approx 80$, and that of the cytosol is $\epsilon_c \approx 80$.

We use the method of image charges. The charge q at $(0,0,h)$ for $-t/2 < h < t/2$ will generate image charges at the points $\boldsymbol{r} = (0,0,2nt+h)$ and $\boldsymbol{r} = (0,0,(2n+1)t-h)$ in which n runs over all the integers. The cylindrical symmetry of the problem ensures that the potential is independent of the azimuthal angle ϕ and so can depend only upon $\rho = \sqrt{x^2+y^2}$ and z. The details of the calculation are relegated to the Appendix.

As shown there, the electrostatic potential in the lipid bilayer $V_\ell(\rho,z)$ due to a charge q in the lipid bilayer at the point $(0,0,h)$ on the z-axis is

$$V_\ell(\rho,z) = \frac{q}{4\pi\epsilon_0\epsilon_\ell}\left[\sum_{n=-\infty}^{\infty}\frac{(pp')^n}{\sqrt{\rho^2+(z-2nt-h)^2}} - \sum_{n=0}^{\infty}\frac{p\,(pp')^n}{\sqrt{\rho^2+(z-(2n+1)t+h)^2}} - \sum_{n=1}^{\infty}\frac{p'\,(pp')^{n-1}}{\sqrt{\rho^2+(z+(2n-1)t+h)^2}}\right] \quad (8)$$

in which p and p' are the ratios

$$p = \frac{\epsilon_w-\epsilon_\ell}{\epsilon_w+\epsilon_\ell} \quad \text{and} \quad p' = \frac{\epsilon_c-\epsilon_\ell}{\epsilon_c+\epsilon_\ell} \quad (9)$$

which lie between 0 and 1.

That in the extra-cellular medium is

$$V_w(\rho,z) = \frac{q}{4\pi\epsilon_0\epsilon_{w\ell}}\left[\sum_{n=0}^{\infty}\frac{(pp')^n}{\sqrt{\rho^2+(z+2nt-h)^2}} - \sum_{n=1}^{\infty}\frac{p'\,(pp')^{n-1}}{\sqrt{\rho^2+(z+(2n-1)t+h)^2}}\right] \quad (10)$$

where $\epsilon_{w\ell} = (\epsilon_w+\epsilon_\ell)/2$ is average of relative permittivity of the extracellular medium ϵ_w and that of the lipid bilayer ϵ_ℓ.

Finally, the potential in the cytosol is

$$V_c(\rho,z) = \frac{q}{4\pi\epsilon_0\epsilon_{c\ell}}\left[\sum_{n=0}^{\infty}\frac{(pp')^n}{\sqrt{\rho^2+(z-2nt-h)^2}} - \frac{p\,(pp')^n}{\sqrt{\rho^2+(z-(2n+1)t+h)^2}}\right] \quad (11)$$

in which $\epsilon_{c\ell} = (\epsilon_c+\epsilon_\ell)/2$ is average of relative permittivity of the cytosol ϵ_c and that of the lipid bilayer ϵ_ℓ.

The first 1000 terms of the series (8), (10), & (11) for the potentials $V_\ell(\rho,z)$, $V_w(\rho,z)$, and $V_c(\rho,z)$ are plotted in Fig. 1 (in Volts) for $\rho = 1$ nm as a function of the height z (nm) above the midpoint of the phospholipid bilayer for a unit charge $q = |e|$ in the bilayer at $(\rho,z) = (0,-2)$ (left curve, blue), $(0,0)$ (middle curve, green), and $(0,2)$ nm (right curve, red). The lipid bilayer extends from $z = -2.5$ to $z = 2.5$ nm and is bounded by black vertical lines in the figure. The cytosol lies below $z = -2.5$ nm. The relative permittivities were taken to be $\epsilon_w = \epsilon_c = 80$ and $\epsilon_\ell = 2$.

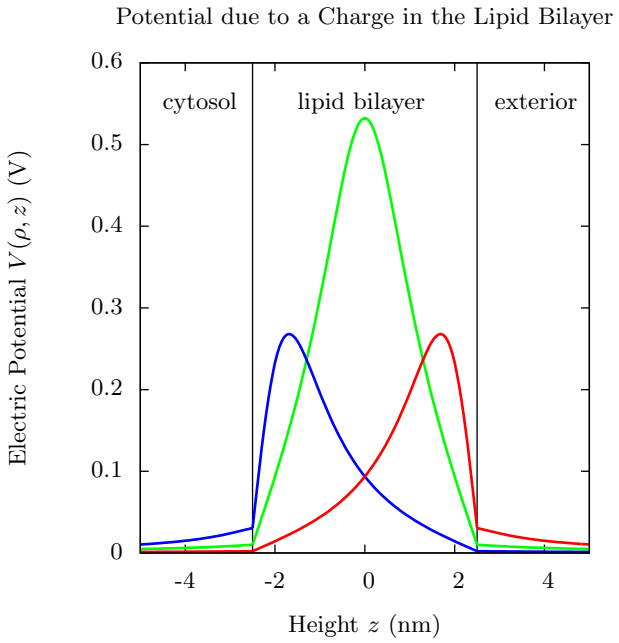

FIG. 1: The electric potential $V(\rho,z)$ from (8–11) in Volts for $\rho = 1$ nm as a function of the height z (nm) above the midpoint of the phospholipid bilayer for a unit charge $q = |e|$ in the phospholipid bilayer at $(\rho,z) = (0,-2)$ nm (left, blue), $(0,0)$ (middle, green), and $(0,2)$ nm (right, red). The lipid bilayer extends from $z = -2.5$ to $z = 2.5$ nm, and is bounded by black vertical lines in the figure. The relative permittivities are taken to be $\epsilon_w = \epsilon_c = 80$ and $\epsilon_\ell = 2$.

III. THE POTENTIAL DUE TO A CHARGE IN THE EXTRACELLULAR MEDIUM

In Appendix A of [3], I calculated the electrostatic potential due to a charge in the extracellular medium by using the asymmetrical coordinates $z' = z - t/2$ and $h' = h - t/2$ used in the Appendix of the present paper. Transforming those formulas to the symmetrical coordinates z and h, we see that the potential in the lipid bilayer $V_\ell(\rho,z)$ due to a charge q in the extra-cellular environment at the point $(0,0,h)$ on the z-axis a height h above the midline of the lipid bilayer is

$$V_\ell(\rho,z) = \frac{q}{4\pi\epsilon_0\epsilon_{w\ell}}\sum_{n=0}^{\infty}\left[\frac{(pp')^n}{\sqrt{\rho^2+(z-2nt-h)^2}} - \frac{p'(pp')^n}{\sqrt{\rho^2+(z+(2n+1)t+h)^2}}\right]. \quad (12)$$

The potential in the extracellular medium is

$$V_w(\rho,z) = \frac{q}{4\pi\epsilon_0\epsilon_w}\left[\frac{1}{r}+\frac{p}{\sqrt{\rho^2+(z-t+h)^2}} - \frac{\epsilon_w\epsilon_\ell}{\epsilon_{w\ell}^2}\sum_{n=1}^{\infty}\frac{p^{n-1}p'^n}{\sqrt{\rho^2+(z+(2n-1)t+h)^2}}\right] \quad (13)$$

in which $r = \sqrt{\rho^2+(z-h)^2}$ is the distance from the charge q.

The potential in the cytosol due to the same charge q is

$$V_c(\rho,z) = \frac{q\,\epsilon_\ell}{4\pi\epsilon_0\epsilon_w\epsilon_\ell\epsilon_{c\ell}}\sum_{n=0}^{\infty}\frac{(pp')^n}{\sqrt{\rho^2+(z-2nt-h)^2}}. \quad (14)$$

The first 1000 terms of the series (12), (13), & (14) for the potentials $V_\ell(\rho,z)$, $V_w(\rho,z)$, and $V_c(\rho,z)$ are plotted in Fig. 2 (in Volts) for $\rho = 1$ nm as a function of the height z (nm) above the midpoint of the phospholipid bilayer for a unit charge $q = |e|$ in the extracellular medium at $(\rho,z) = (0, 3.5)$ nm (right curve, red). The lipid bilayer extends from $z = -2.5$ to $z = 2.5$ nm, and the cytosol lies below $z = -2.5$ nm. The relative permittivities were taken to be $\epsilon_w = \epsilon_c = 80$ and $\epsilon_\ell = 2$.

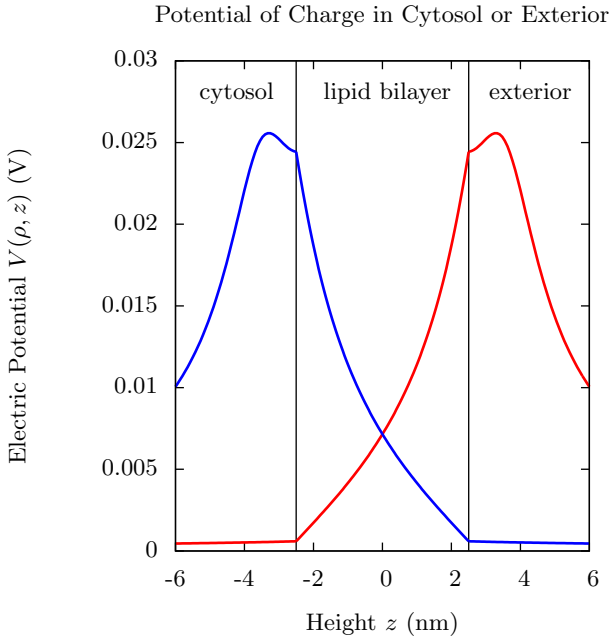

FIG. 2: The electric potential $V(\rho,z)$ from (12–14) and (15–17) in Volts for $\rho = 1$ nm as a function of the height z (nm) above or below the midpoint of the phospholipid bilayer for a unit charge $q = |e|$ in the cytosol at $(\rho,z) = (0,-3.5)$ nm (left curve, blue) and in the extracellular medium at $(0, 3.5)$ nm (right curve, red). The lipid bilayer and the relative permittivities are as in Fig 1.

IV. THE POTENTIAL DUE TO A CHARGE IN THE CYTOSOL

We may find the potential due to a charge in the cytosol by a symmetry argument from the potential due to a charge in the extracellular medium. Thus, $V_w(\rho,z)$ for a charge in the cytosol at $\boldsymbol{r} = (0,0,h)$ with $h \le -t/2$ is $V_c(\rho,-z)$ for a charge in the extra-cellular medium at $\boldsymbol{r} = (0,0,-h)$. Similarly, $V_c(\rho,z)$ for a charge in the cytosol at $(0,0,h)$ with $h \le -t/2$ is $V_w(\rho,-z)$ for a charge in the extra-cellular medium at $\boldsymbol{r} = (0,0,-h)$ but with ϵ_ℓ and ϵ_w interchanged. And $V_\ell(\rho,z)$ for a charge in the cytosol at $(0,0,h)$ with $h \le -t/2$ is $V_\ell(\rho,-z)$ for a charge in the extra-cellular medium at $\boldsymbol{r} = (0,0,-h)$ but with ϵ_ℓ and ϵ_w as well as p and p' interchanged.

Thus, the potential in the lipid bilayer is

$$V_\ell(\rho,z) = \frac{q}{4\pi\epsilon_0\epsilon_{c\ell}}\sum_{n=0}^{\infty}\left[\frac{(pp')^n}{\sqrt{\rho^2+(z+2nt-h)^2}} - \frac{p\,(pp')^n}{\sqrt{\rho^2+(z-(2n+1)t+h)^2}}\right] \quad (15)$$

while that in the extra-cellular medium is

$$V_w(\rho,z) = \frac{q\epsilon_\ell}{4\pi\epsilon_0\epsilon_{w\ell}\epsilon_{c\ell}}\sum_{n=0}^{\infty}\frac{(pp')^n}{\sqrt{\rho^2+(z+2nt-h)^2}} \quad (16)$$

and that in the cytosol is

$$V_c(\rho,z) = \frac{q}{4\pi\epsilon_0\epsilon_c}\left[\frac{1}{r}+\frac{p'}{\sqrt{\rho^2+(z+t+h)^2}} - \frac{\epsilon_c\epsilon_\ell}{\epsilon_{c\ell}^2}\sum_{n=1}^{\infty}\frac{p\,(pp')^{n-1}}{\sqrt{\rho^2+(z-(2n-1)t+h)^2}}\right] \quad (17)$$

in which $r = \sqrt{\rho^2+(z-h)^2}$ is the distance to the charge.

The first 1000 terms of the series (15), (16), & (17) for the potentials $V_\ell(\rho,z)$, $V_w(\rho,z)$, and $V_c(\rho,z)$ are plotted in Fig. 2 (in Volts) for $\rho = 1$ nm as a function of the height z (nm) above the midpoint of the phospholipid bilayer for a unit charge $q = |e|$ in the cytosol at $(\rho,z) = (0, -3.5)$ nm (left curve, blue). The lipid bilayer extends from $z = -2.5$ to $z = 2.5$ nm, and the cytosol lies below $z = -2.5$ nm. The relative permittivities were taken to be $\epsilon_w = \epsilon_c = 80$ and $\epsilon_\ell = 2$.

Naively, one might think that the electrostatic potential $V(\rho,z)$ due to a charge at $(0,z_0)$ would have a maximum at $z_{\max} = z_0$ independent of rho. Actually, the formulas of this paper show that the maximum depends upon ρ and is at $z_{\max} = z_0$ only for $\rho = 0$. At finite ρ, the maximum is closer to the midpoint of the lipid bilayer, $|z_{\max}| < |z_0|$ as shown in Fig. 3.

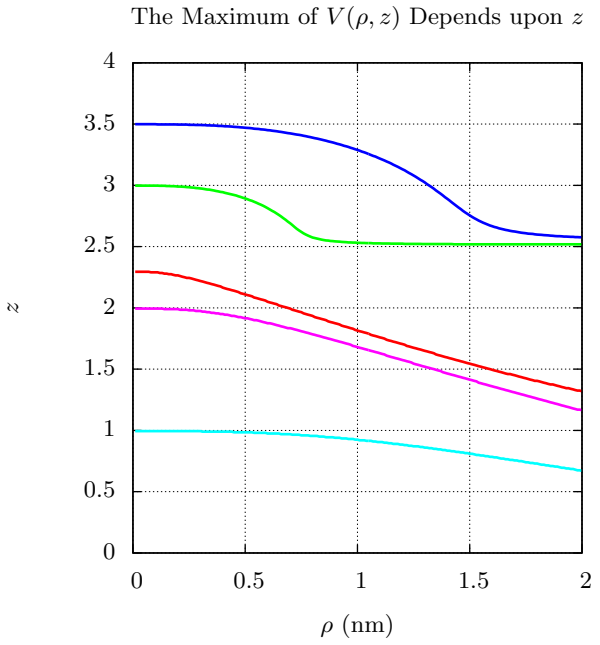

FIG. 3: The maximum of the electric potential $V(\rho, z)$ from (8–17) in Volts for $0 < \rho < 2$ nm as a function of the height z (nm) above the midpoint of the phospholipid bilayer for a unit charge $q = |e|$ at $(\rho, z) = (0, 3.5)$ nm (top curve, blue), $(0, 3)$ nm (second curve, green), $(0, 2.3)$ nm (third curve, red), $(0, 2)$ nm (fourth curve, purple), and $(0, 1)$ nm (bottom curve, cyan). The maximum in $V(\rho, z)$ due to a charge at z_0 occurs at a value of $z = z_{\max}$ that is closer than z_0 to the midpoint of the lipid bilayer, that is, $|z_{\max}| < |z_0|$. The lipid bilayer and the relative permittivities are as in Fig. 1.

V. ELECTROPORATION

Electroporation is the formation of pores in membranes by an electric field. Depending on the duration of the field and the type of cell, an electric potential difference across a cell's plasma membrane in excess of 150 to 200 mV will create pores. There are two main components to the energy of a pore. The first is the line energy $2\pi r\gamma$ due to the linear tension γ, which is of the order of 10^{-11} J/m. The second is the electrical energy which is the difference ΔW between the energy

$$W = \frac{\epsilon_0 \epsilon_\ell}{2} \int \boldsymbol{E}^2(\boldsymbol{x})\, d^3x. \tag{18}$$

when the pore is made of lipid and when it is made of saline water. This energy change usually is taken to be $\Delta W = -0.5\Delta C \pi r^2 (\Delta V)^2$ in which ΔV is the voltage across the membrane and $\Delta C = C_w - C_\ell$ is the difference between the specific capacity per unit area $C_w = \epsilon_w \epsilon_0 / t$ of the water-filled pore and that $C_\ell = \epsilon_\ell \epsilon_0 / t$ of the pore-free membrane of thickness t. There also is a small term due to the surface tension Σ of the plasma membrane of the cell, but this term usually is negligible since Σ is of the order of 2.5×10^{-6} J/m^2 [4]. The energy of the pore in a plasma membrane is then [5–9]

$$E(r) = 2\pi r\gamma - \pi r^2 \Sigma - \tfrac{1}{2}\pi r^2 \Delta C\, (\Delta V)^2. \tag{19}$$

This energy has a maximum of

$$E(r_c) = \frac{\pi \gamma^2}{\Sigma + \frac{1}{2}\Delta C (\Delta V)^2} \approx \frac{2\pi\gamma^2}{\Delta C (\Delta V)^2} \tag{20}$$

at the critical radius

$$r_c = \frac{\gamma}{\Sigma + \frac{1}{2}\Delta C\, (\Delta V)^2} \approx \frac{2\gamma}{\Delta C\, (\Delta V)^2}. \tag{21}$$

In Fig. 4, the Boltzmann factor $e^{-E(r)/(kT)}$ ($\times 100$) is plotted as a function of the radius r of the pore up to the critical radius r_c for various transmembrane voltages from -200 (solid, red) to -400 mV (dot-dash, cyan). Clearly, the chance of a pore forming rises steeply with the magnitude of the voltage and falls with the radius of the pore.

If the transmembrane potential ΔV is turned off before the radius of the pore reaches r_c, then the radius r of the pore usually shrinks quickly (well within 1 ms [6]) to a radius so small as to virtually shut-down the conductivity of the pore. This rapid closure occurs because in (19) the energy $2\pi r\gamma$ dominates over $-\pi r^2 \Sigma$, the surface tension Σ being negligible. Such a pore is said to be reversible. But if ΔV remains on when r exceeds the critical radius r_c, then the pore usually will grow and lyse the cell; such a pore is said to be irreversible.

The formula (21) provides an upper limit on the radius of a reversible pore. This upper limit drops with the square of the transmembrane voltage ΔV from $r_c = 3.6$ nm for $\Delta V = -200$ mV, to 1.6 nm for $\Delta V = -300$, and to 0.9 nm for $\Delta V = -400$ mV.

The time t_ℓ for a pore's radius to reach the critical radius r_c is the time to lysis; it varies greatly and apparently randomly even within cells of a given kind. In erythrocytes, its mean value drops by nearly an order of magnitude with each increase of 100 mV in the transmembrane potential [6] and is about a fifth of a second when $\Delta V = -300$ mV.

Electroporation may be part of the physics behind the transduction of cell-penetrating peptides and the exocytosis of neurotransmitters, as explained in Sections VI & VII.

VI. MOLECULAR ELECTROPORATION AND THE TRANSDUCTION OF OLIGOARGININES

Cell-penetrating peptides (CPPs) can carry into cells cargoes with molecular weights of as much as 3,000 Da—much greater than the nominal limit 500 of the "rule of 5" [10]. Therapeutic applications with well-chosen peptide cargoes of 8–33 amino acids are described in references [11–23].

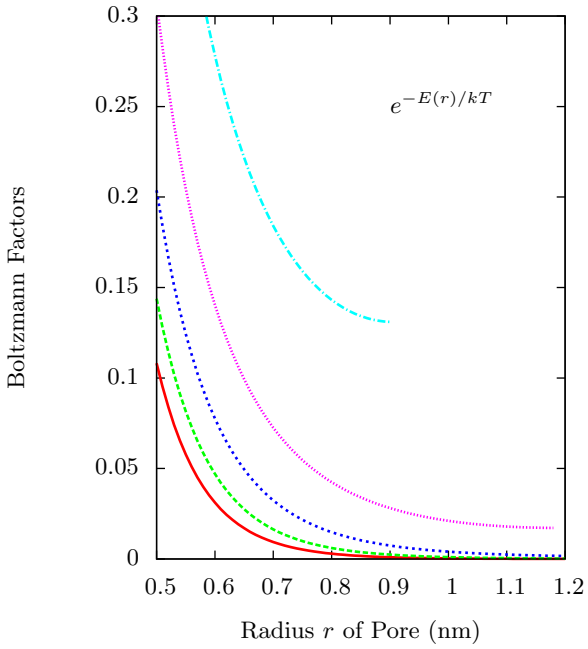

FIG. 4: The Boltzmann factor $e^{-E(r)/kT}$ ($\times 100$) for energy $E(r)$ (Eq.(19)) is plotted against the radius r of the pore up to the critical radius r_c (Eq.(21)) for the transmembrane voltage $\Delta V = -200$ (solid red), -250 (dashes green), -300 (dots blue), -350 (dots magenta), and -400 mV (dash-dot cyan). The curves stop at the critical radius r_c beyond which the pores expand irreversibly.

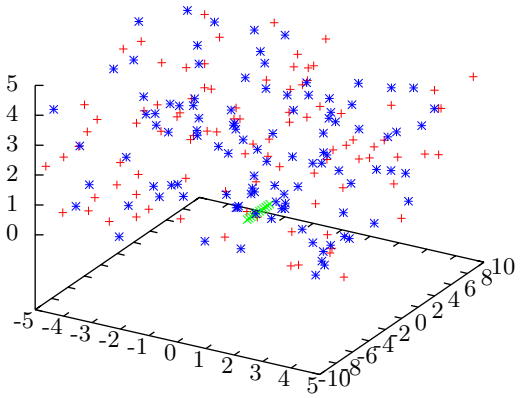

FIG. 5: Snapshot of 94 sodium ions (pluses, red), 106 chloride ions (stars, blue), and a 12-mer random coil of oligoarginine R^{12} (x's, green) after 50,000 sweeps. The coordinates are in nm.

In a model advanced in references [3, 24, 25], a polyarginine sticks to the cell membrane as its guanidinium groups electrostatically interact with the phosphate groups of the outer leaflet of the phospholipid bilayer. If the positive charge of the polyarginine exceeds about $8|e|$, then it can raise the transmembrane potential above the threshold for electroporation, some -200 mV [4–9].

The transmembrane potential ΔV is the sum of three terms

$$\Delta V = \Delta V_{cell} + \Delta V_{CPP} + \Delta V_{NaCl} \tag{22}$$

the resting transmembrane potential ΔV_{cell} of the cell in the absence of CPPs, the transmembrane potential ΔV_{CPP} due to an oligoarginine or other CPP, and the transmembrane potential ΔV_{NaCl} due to the counterions of the extracellular medium. The resting transmembrane potential ΔV_{cell} of the cell varies between about 20 mV to more than 70 mV, depending upon the type of cell. Ideally, it is measured experimentally. The transmembrane potential ΔV_{CPP} due to an oligoarginine or to some other positively charged CPP may be determined from the formulas (12–14) for the potential of a charge outside a membrane [3]. The transmembrane potential ΔV_{NaCl} due to the counterions of the extracellular medium requires a Monte Carlo simulation of the Na^+, Cl^-, and other ions of the extracellular medium in the electrostatic potential $V_{cell} + V_{CPP}$. This simulation was performed in [3] with the aid of equations (12–14).

The code took snapshots of the distributions of the sodium and chloride ions every 2500 sweeps after thermalization. Fig. 5 displays the last snapshot (after 50,000 sweeps) of 94 Na^+, 106 Cl^-, and 12 Rs in a random coil. The coordinates are in nm.

The lipid bilayer insulates the extracellular counterions from the potential due to the counterions of the cytosol, however, so their potential may be neglected in the simulation of the extracellular counterions.

The values of $\Delta V_{CPP} + \Delta V_{NaCl}$ found in Monte Carlo simulations [3] of the salt around an R^N oligoarginine are listed in Table I. A resting transmembrane potential $-120 < \Delta V_{cell} < -20$ mV should be added to these values of $\Delta V_{CPP} + \Delta V_{NaCl}$ to obtain the full transmembrane potential ΔV. For $N > 8$, the transmembrane potential ΔV can exceed -200 mV which is enough [4–9] to cause electroporation in common eukaryotic cells.

In references [24] and [3], it was pointed out that one way to test the model advanced in those papers would be to look for the formation of reversible pores by detecting transient (ms) changes in the conductance of membranes exposed to CPPs such as R^9. Such experiments have now been done. Using the planar-phospholipid-bilayer method, Herce *et al.* found that R^9 induced transient ionic currents through model phospholipid membranes [26]. They estimated that the mean radius of these pores to be 0.66 nm, which is safely below the limiting critical radius (21) of between 0.9 and 3.6 nm for the voltage range of $-400 \le \Delta V \le -200$ mV. Moreover, using the patch-clamp technique, they found that R^9 induced transient ionic currents through the mem-

TABLE I: The voltage differences $\Delta V_{CPP} + \Delta V_{NaCl}$ (mV) across the plasma membrane induced by an R^N oligoarginine as an α-helix, a random coil, or a β-strand and by the ions of 156 mM Na^+ and Cl^- reacting to it. The resting transmembrane potential ΔV_{cell} is not included.

N	R^N α-helix	R^N random coil	R^N β-strand
5	-144 ± 4	-154 ± 3	-148 ± 4
6	-174 ± 4	-173 ± 4	-168 ± 1
7	-206 ± 4	-201 ± 3	-189 ± 2
8	-232 ± 3	-228 ± 1	-199 ± 5
9	-256 ± 6	-246 ± 2	-205 ± 4
10	-281 ± 2	-260 ± 5	-210 ± 4
11	-306 ± 5	-260 ± 3	-218 ± 4
12	-323 ± 4	-261 ± 4	-213 ± 2

branes of both freshly isolated human umbilical-artery (HUA) smooth-muscle cells and cultured osteosarcoma cells [26]. These experimental confirmations of the predictions made in references [24] and [3] lend some support to the model advanced in these papers and sketched in this subsection, but they do not prove that it is correct. It is, in any case, a continuum model of a molecular effect, and it may be consistent with the one simulated in reference [26].

VII. MOLECULAR ELECTROPORATION AND THE EXOCYTOSIS OF NEUROTRANSMITTERS

A synaptic terminal of an axon is crowded with vesicles loaded with neurotransmitters, usually glutamate (exitatory) and its close relative GABA (inhibitory). Some 5 to 10 vesicles wait near its plasma membrane poised to fuse with that bilayer and release their neurotransmitters.

The arrival of an action potential opens voltage-gated calcium channels and allows an influx of Ca^{2+} ions into the cytosol of the presynaptic axon. At least 3 calcium-sensitive synaptotagmin/SNARE (syt-t-SNARE) complexes [28] attach each vesicle to the axon's plasma membrane as shown in Fig. 6. After the influx of calcium, each synaptotagmin (syt) binds 3 Ca^{2+} ions in its C2A calcium-binding region and another 2 in its C2B binding domain. When 3 syt-t-SNARE complexes bind 15 Ca^{2+} ions, they increase the charge around the junction of the vesicle with the axon membrane by $30|e|$. This huge change is enough to alter the shape of the syt-t-SNARE complexes and to insert the Ca^{2+} ions into the plasma membrane of the axon [27] as shown in Fig. 6. The shape change causes the vesicle to hemifuse its distal membranes with those of the plasma membrane. The electrostatic change enhances the probability of molecular electroporation—the formation of a pore of saline water leading from the interior of the vesicle through the hemifused vesicle-axon bilayer to the synaptic cleft. A voltage drop of about 200 mV across a plasma membrane

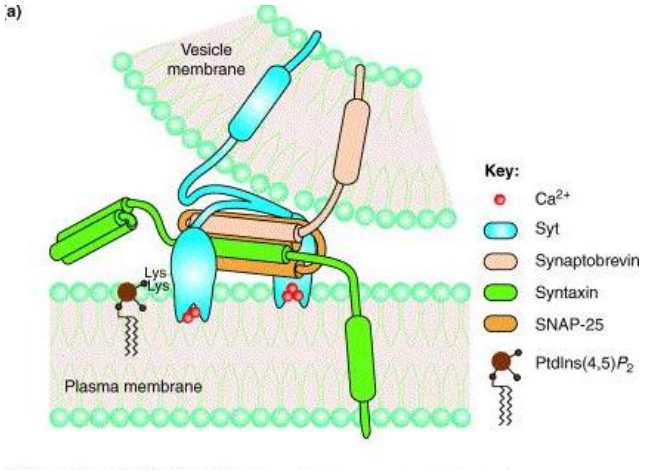

FIG. 6: Model of the Ca2+-activated membrane fusion complex. (a) In the presence of Ca2+, the Ca2+-binding loops of both the C2A and C2B domains of synaptotagmin I (syt) insert into the bilayer [15]. Phosphatidyl inositol 4,5-bisphosphate [PtdIns(4,5)P2] (localized on the inner leaflet of the target membrane) steers the membrane penetration activity of the C2 domains towards the target membrane [12]. These interactions bring the opposing bilayers into close proximity. Furthermore, syt directly interacts with isolated target membrane SNAREs (t-SNAREs), binary t-SNARE complexes, and assembled ternary SNARE complexes. Syt-t-SNARE interactions might connect the Ca2+-sensing process directly to membrane fusion by regulating the assembly of trans-SNARE complexes and/or the disposition of SNARE complexes during the opening and dilation of fusion pores. Abbreviation: SNAP-25, synaptosome-associated protein of 25 kDa. Figure from [27], used with the permission of E. R. Chapman and Elsevier.

is enough for molecular electroporation.

Fig. 7 shows the electrostatic potential $V(\rho, z)$ at $\rho = 1$ nm due to a unit charge $|e|$ on the z-axis at $\rho = 0$ just Ångströms inside the lipid bilayer at $(\rho, z) = (0, t/2 - n\text{Å})$ for $n = 3$ (top curve, blue), $n = 2$ (middle curve, green), and $n = 1$ (bottom curve, red). Note that $\rho = 1$ nm, the maximum in $V(\rho, z)$ due to a charge at z_0 occurs at a value of $z = z_{\max}$ that is closer than z_0 to the midpoint of the lipid bilayer, that is, $|z_{\max}| < |z_0|$, as illustrated in Fig. 3. Thus, the charges are much closer to the lipid-exterior interface than they appear to be in Fig. 7.

Since the volume integral (18) of the electric permittivity times the square of the electric field determines the energy advantage of electroporation, the effective voltage V_{eff} is the sum of the absolute value of the change in the potential $V(\rho, z)$ from $z = t/2$ to its maximum at $z = z_{\max}$ and the absolute value of the change in the potential $V(\rho, z)$ from that maximum to $z = -t/2$

$$V_{\text{eff}} = |V(\rho, z_{\max}) - V(\rho, t/2)| + |V(\rho, z_{\max}) - V(\rho, -t/2)|. \quad (23)$$

Thus, the effective voltage V_{eff} is about 130 mV for a unit charge $|e|$ at $z_0 = 2.4$ nm and about 320 mV for one at $z_0 = 2.2$. The C2A domain of syt uses 5 aspartates

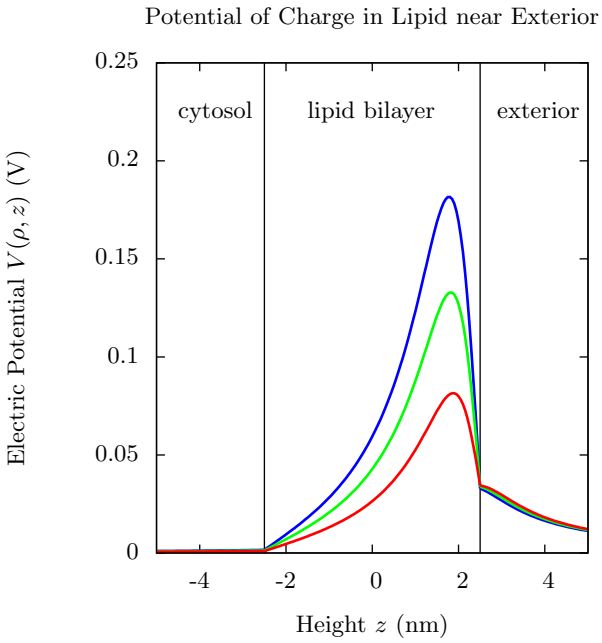

FIG. 7: The electric potential $V(\rho,z)$ from (8–11) in Volts for $\rho = 1$ nm as a function of the height z (nm) above the midpoint of the phospholipid bilayer for a unit charge $q = |e|$ just inside the lipid bilayer at $(\rho,z) = (0,2.2)$ nm (left curve, blue), $(\rho,z) = (0,2.3)$ nm (middle curve, green), and at $(\rho,z) = (0,2.4)$ nm (right curve, red). At $\rho = 1$ nm, the maximum in $V(\rho,z)$ due to a charge at z_0 occurs at a value of $z = z_{\max}$ that is closer than z_0 to the midpoint of the lipid bilayer, that is, $|z_{\max}| < |z_0|$. The lipid bilayer and the relative permittivities are as in Fig. 1.

to bind 3 Ca^{2+} ions, and its C2B domain uses 4 Asps to bind 2 Ca^{2+} ions. So 3 syt-t-SNARE complexes insert a net charge of $3|e|$ into the lipid bilayers of the vesicle and the axon [27].

During an action potential, pore formation in a single vesicle occurs with low probability, perhaps 0.04, but since there are 5–10 vesicles in attendance, the probability of one of them releasing its neurotransmitters is about 0.3.

If the radius r_p of the pore is $r_p < r_c$ less than the critical radius (21), then the pore collapses with the partial release of the neurotransmitters, a process called "kiss and run." If the pore radius r_p surpasses r_c, the pore continues to expand, and the entire contents of the vesicle are emptied into the synaptic cleft.

VIII. THE NOISY BRAIN

Like any open physical system, the brain lurches to states of minimum free energy. These transitions are constrained by anatomy. They are enabled by sugar and oxygen, by thermal fluctuations, and by stochastic neural events, such as the triggering of an action potential and the release of neurotransmitters into a synaptic cleft. All these forms of noise contribute to an effective temperature. Without such noise, the effective temperature would be zero, and transitions to states of lower free energy, could not occur. Without noise, there is no thought. Bacteria use noise to forage [29, 30].

Appendix: Computation of the Potential

It will be somewhat simpler to use an asymmetrical coordinate system in which $z' \equiv z - t/2 = 0$ denotes the interface between the extracellular medium and the lipid bilayer. In these coordinates, the charge in the bilayer is at $z' = h' \equiv h - t/2$. These coordinates have the advantage that the charge and the image charges are at the points $\boldsymbol{r} = (0,0,2nt \pm h')$ for all integers n.

In this notation, the potential in the lipid bilayer is

$$V_\ell(\rho,z') = \frac{1}{4\pi\epsilon_0\epsilon_\ell}\sum_{s=\pm1}\sum_{n=-\infty}^{\infty}\frac{q_{n,s}}{\sqrt{\rho^2+(z'-(2nt+sh'))^2}} \tag{A.1}$$

while that in the extracellular environment is

$$V_w(\rho,z') = \frac{1}{4\pi\epsilon_0\epsilon_w}\sum_{s=\pm1}\sum_{n=-\infty}^{0}\frac{q_{wn,s}}{\sqrt{\rho^2+(z'-(2nt+sh'))^2}} \tag{A.2}$$

with $q_{w0,-1} = 0$, and that in the cytosol is

$$V_c(\rho,z') = \frac{1}{4\pi\epsilon_0\epsilon_c}\sum_{s=\pm1}\sum_{n=0}^{\infty}\frac{q_{cn,s}}{\sqrt{\rho^2+(z'-(2nt+sh'))^2}}. \tag{A.3}$$

The continuity (4) of the transverse electric field E_ρ and that (5) of the normal displacement $D_{z'}$ across the planes $z' = 0$ and $z' = -t$ imply that the coefficients q_0, $q_{n,s}$, $q_{wn,s}$, and $q_{cn,s}$ must satisfy for $n > 0$ and $s = \pm1$ the relations

$$q_{n,s} + q_{-n,-s} = \frac{\epsilon_\ell}{\epsilon_w}q_{w-n,-s} \tag{A.4}$$

$$q_{n,s} - q_{-n,-s} = -q_{w-n,-s} \tag{A.5}$$

$$q_{n,s} + q_{-(n+1),-s} = \frac{\epsilon_\ell}{\epsilon_c}q_{cn,s} \tag{A.6}$$

$$q_{n,s} - q_{-(n+1),-s} = q_{cn,s} \tag{A.7}$$

as well as the six special cases

$$q_{0,-1} + q_{0,1} = \frac{\epsilon_\ell}{\epsilon_w}q_{w0,1} \tag{A.8}$$

$$q_{0,-1} - q_{0,1} = -q_{w0,1} \tag{A.9}$$

$$q_{0,1} + q_{-1,-1} = \frac{\epsilon_\ell}{\epsilon_c}q_{c0,1} \tag{A.10}$$

$$q_{0,1} - q_{-1,-1} = q_{c0,1} \tag{A.11}$$

$$q_{-1,1} + q_{0,-1} = \frac{\epsilon_\ell}{\epsilon_c}q_{c0,-1} \tag{A.12}$$

$$q_{0,-1} - q_{-1,1} = q_{c0,-1}. \tag{A.13}$$

The four equations (A.4–A.7) tell us that for $n > 0$ and $s = \pm 1$

$$q_{n,s} = -\frac{\epsilon_w - \epsilon_\ell}{2\epsilon_w} q_{w-n,-s} \quad (A.14)$$

$$q_{-n,-s} = \frac{\epsilon_w + \epsilon_\ell}{2\epsilon_w} q_{w-n,-s} \quad (A.15)$$

$$q_{n,s} = \frac{\epsilon_c + \epsilon_\ell}{2\epsilon_c} q_{cn,s} \quad (A.16)$$

$$q_{-(n+1),-s} = -\frac{\epsilon_c - \epsilon_\ell}{2\epsilon_c} q_{cn,s} \quad (A.17)$$

from which we can infer that for $n > 0$

$$q_{n,s} = -p q_{-n,-s} \quad (A.18)$$

and that for $n > 1$ and $s = \pm 1$

$$q_{n,s} = (pp')^{n-1} q_{1,s} \quad (A.19)$$

$$q_{-n,s} = -p^{n-2} p'^{n-1} q_{1,-s} \quad (A.20)$$

$$q_{cn,s} = (1+p')(pp')^{n-1} q_{1,s} \quad (A.21)$$

$$q_{w-n,s} = -(1+p) p^{n-2} p'^{n-1} q_{1,-s} \quad (A.22)$$

in which we used the abbreviations

$$p = \frac{\epsilon_w - \epsilon_\ell}{\epsilon_w + \epsilon_\ell} \quad \text{and} \quad p' = \frac{\epsilon_c - \epsilon_\ell}{\epsilon_c + \epsilon_\ell} \quad (A.23)$$

which lie between 0 and 1.

With the further abbreviations $\epsilon_{w\ell} = (\epsilon_w + \epsilon_\ell)/2$ and $\epsilon_{c\ell} = (\epsilon_c + \epsilon_\ell)/2$, the six relations (A.8–A.13) imply that

$$q_{w0,1} = -\frac{\epsilon_w}{p\epsilon_{w\ell}} q_{0,-1} \quad (A.24)$$

$$q_{w0,1} = \frac{\epsilon_w}{\epsilon_{w\ell}} q_{0,1} \quad (A.25)$$

$$q_{c0,1} = \frac{\epsilon_c}{\epsilon_{c\ell}} q_{0,1} \quad (A.26)$$

$$q_{c0,1} = -\frac{\epsilon_c}{p'\epsilon_{c\ell}} q_{-1,-1} \quad (A.27)$$

$$q_{c0,-1} = \frac{\epsilon_c}{\epsilon_{c\ell}} q_{0,-1} \quad (A.28)$$

$$q_{c0,-1} = -\frac{\epsilon_c}{p'\epsilon_{c\ell}} q_{-1,1} \quad (A.29)$$

Gauss's law (1) applied to a tiny sphere about the physical charge q gives

$$q_{0,1} = q. \quad (A.30)$$

This identification and the six equations (A.24–A.29) tell us that

$$q_{w0,1} = \frac{\epsilon_w}{\epsilon_{w\ell}} q \quad (A.31)$$

$$q_{c0,1} = \frac{\epsilon_c}{\epsilon_{c\ell}} q \quad (A.32)$$

$$q_{0,-1} = -p q \quad (A.33)$$

$$q_{-1,-1} = -p' q \quad (A.34)$$

$$q_{c0,-1} = -p\frac{\epsilon_c}{\epsilon_{c\ell}} q \quad (A.35)$$

$$q_{-1,1} = pp' q. \quad (A.36)$$

Equations (A.18–A.36) allow us to relate all the coefficients for $n > 0$ to $q_{0,1} = q$ and to $q_{w0,-1} = 0$:

$$q_{n,1} = (pp')^n q \quad (A.37)$$

$$q_{n,-1} = -p(pp')^n q \quad (A.38)$$

$$q_{-n,1} = (pp')^n q \quad (A.39)$$

$$q_{-n,-1} = -p'(pp')^{n-1} q \quad (A.40)$$

$$q_{w-n,1} = (1+p)(pp')^n q \quad (A.41)$$

$$q_{w-n,-1} = -(1+p)p'(pp')^{n-1} q \quad (A.42)$$

$$q_{cn,1} = (1+p')(pp')^n q \quad (A.43)$$

$$q_{cn,-1} = -(1+p')p(pp')^n q. \quad (A.44)$$

The electric potential due to a charge q in the lipid bilayer of thickness t and a distance $|h'| = -h'$ below the extra-cellular environment then is

$$V_\ell(\rho, z') = \frac{q}{4\pi\epsilon_0\epsilon_\ell}\left[\sum_{n=-\infty}^{\infty}\frac{(pp')^n}{\sqrt{\rho^2+(z'-2nt-h')^2}} - \sum_{n=0}^{\infty}\frac{p(pp')^n}{\sqrt{\rho^2+(z'-2nt+h')^2}} - \sum_{n=1}^{\infty}\frac{p'(pp')^{n-1}}{\sqrt{\rho^2+(z'+2nt+h')^2}}\right] \quad (A.45)$$

in the lipid bilayer. That in the extra-cellular environment is

$$V_w(\rho, z') = \frac{q}{4\pi\epsilon_0\epsilon_{w\ell}}\left[\sum_{n=0}^{\infty}\frac{(pp')^n}{\sqrt{\rho^2+(z'+2nt-h')^2}} - \sum_{n=1}^{\infty}\frac{p'(pp')^{n-1}}{\sqrt{\rho^2+(z'+2nt+h')^2}}\right]. \quad (A.46)$$

Finally, the potential in the cytosol is

$$V_c(\rho, z') = \frac{q}{4\pi\epsilon_0\epsilon_{c\ell}}\left[\sum_{n=0}^{\infty}\frac{(pp')^n}{\sqrt{\rho^2+(z'-2nt-h')^2}} - \frac{p(pp')^n}{\sqrt{\rho^2+(z'-2nt+h')^2}}\right]. \quad (A.47)$$

We now revert to our symmetrical coordinates in which $z = z' + t/2$ and $h = h' + t/2$. The electric potential due to a charge q in the lipid bilayer of thickness t at $\boldsymbol{r} = (0, 0, h)$ where $-t/2 \le h \le t/2$ now is

$$V_\ell(\rho, z) = \frac{q}{4\pi\epsilon_0\epsilon_\ell}\left[\sum_{n=-\infty}^{\infty}\frac{(pp')^n}{\sqrt{\rho^2+(z-2nt-h)^2}} - \sum_{n=0}^{\infty}\frac{p(pp')^n}{\sqrt{\rho^2+(z-(2n+1)t+h)^2}} - \sum_{n=1}^{\infty}\frac{p'(pp')^{n-1}}{\sqrt{\rho^2+(z+(2n-1)t+h)^2}}\right] \quad (A.48)$$

in the lipid bilayer. The potential in the extra-cellular environment is

$$V_w(\rho,z) = \frac{q}{4\pi\epsilon_0\epsilon_{w\ell}}\left[\sum_{n=0}^{\infty}\frac{(pp')^n}{\sqrt{\rho^2+(z+2nt-h)^2}} - \sum_{n=1}^{\infty}\frac{p'\,(pp')^{n-1}}{\sqrt{\rho^2+(z+(2n-1)t+h)^2}}\right] \quad \text{(A.49)}$$

Finally, the potential in the cytosol is

$$V_c(\rho,z) = \frac{q}{4\pi\epsilon_0\epsilon_{c\ell}}\left[\sum_{n=0}^{\infty}\frac{(pp')^n}{\sqrt{\rho^2+(z-2nt-h)^2}} - \frac{p\,(pp')^n}{\sqrt{\rho^2+(z-(2n+1)t+h)^2}}\right]. \quad \text{(A.50)}$$

To check that these formulas for the electrostatic potentials give rise to a transverse electric field E_ρ and a normal electric displacement D_z that are continuous across the water-lipid and lipid-cytosol interfaces, I wrote two codes defs.f90 and checks.f90 that are publicly available online [31].

Acknowledgments

I am particularly grateful to Michael Wilson for several conversations about the exocytosis of neurotransmitters. I also am grateful to Samantha Schwartz, Toby Tolley, and Vaibhav Madhok for their comments, to Leonid Chernomordik for tips about electroporation, to Gisela Tünnemann for sharing her data, to Sergio Hassan for advice about the NaCl potential, to Pavel Jungwirth for advice on guanidinium groups, to John Connor and Karlheinz Hilber for explaining the status of measurements of the membrane potential of mouse myoblast cells, to Paul Robbins for sending me some of his images, to Jean Vance for information about mammalian cells deficient in the synthesis of phosphatidylserine, and to James Thomas for several useful conversations. Thanks also to H. Berg, S. Bezrukov, H. Bryant, P. Cahill, D. Cromer, G. Herling, T. Hess, S. Koch, V. Madhok, M. Malik, A. Parsegian, B. B. Rivers, K. Thickman, and T. Tolley for useful conversations, and to K. Dill, S. Dowdy, S. Henry, K. Hilber, A. Pasquinelli, B. Salzberg, D. Sergatskov, L. Sillerud, A. Strongin, R. Tsien, J. Vance, and A. Ziegler for helpful e-mail.

[1] Bevers, E., P. Comfurius, D. Dekkers, and R. Zwaal, 1999. Lipid translocation across the plasma membrane of mammalian cells. *Biochim Biophys Acta* 1439(3):317–30.

[2] Alberts, B., A. Johnson, J. Lewis, M. Raff, K. Roberts, and P. Walter, 2002. Molecular Biology of the Cell, Garland Science, New York, 587–593. 4 edition.

[3] Cahill, K. E., 2010. Molecular Electroporation and the Transduction of Oligoarginines. *Phys. Biol.* 7:016001(14pp).

[4] Dai, J., H. P. Ting-Beall, and M. P. Sheetz, 1997. The Secretion-coupled Endocytosis Correlates with Membrane Tension Changes in RBL 2H3 Cells. *J. Gen. Physiol.* 110(1):1–10.

[5] Abidor, I. G., V. B. Arakelyan, L. V. Chernomordik, Y. A. Chizmadzhev, V. F. Pastushenko, and M. R. Tarasevich, 1979. Electric Breakdown of Bilayer Lipid Membranes I. The Main Experimental Facts and Their Qualitative Discussion. *Bioelectrochem. Bioenerg.* 6:37–52.

[6] Chernomordik, L. V., S. I. Sukharev, S. V. Popov, V. F. Pastushenko, A. V. Sokirko, I. G. Abidor, and Y. A. Chizmadzhev, 1987. The electrical breakdown of cell and lipid membranes: the similarity of phenomenologies. *Bioch. Biophys. Acta* 902:360–373.

[7] Glaser, R. W., S. L. Leikin, L. V. Chernomordik, V. F. Pastushenko, and A. V. Sokirko, 1988. Reversible electrical breakdown of lipid bilayers: formation and evolution of pores. *Bioch. Biophys. Acta* 940:275–287.

[8] Weaver, J., and Y. Chizmadzhev, 1996. Theory of electroporation: A review. *Bioelectrochemistry and Bioenergetics* 41:135–160. `http://dx.doi.org/10.1016/S0302-4598(96)05062-3`.

[9] Melikov, K. C., V. A. Frolov, A. Shcherbakov, A. V. Samsonov, Y. A. Chizmadzhev, and L. V. Chernomordik, 2001. Voltage-Induced Nonconductive Pre-Pores and Metastable Single Pores in Unmodified Planar Lipid Bilayers. *Biophys. J.* 80:1829–1836.

[10] Lipinski, C., F. Lombardo, B. Dominy, and P. Feeney, 1997. Experimental and computational approaches to estimate solubility and permeability in drug discovery and development settings. *Adv. Drug Deliv. Rev.* 23:3–25.

[11] Jiang, T., E. S. Olson, Q. T. Nguyen, M. Roy, P. A. Jennings, and R. Y. Tsien, 2004. Tumor imaging by means of proteolytic activation of cell-penetrating peptides. *Proc. Natl. Acad. Sci. USA* 101(51):17867–17872.

[12] Snyder, E., C. Saenz, C. Denicourt, B. Meade, X. Cui, I. Kaplan, and S. Dowdy, 2005. Enhanced targeting and killing of tumor cells expressing the CXC chemokine receptor 4 by transducible anticancer peptides. *Cancer Res.* 65(23):10646–50.

[13] Willam, C., N. Masson, Y.-M. Tian, S. A. Mahmood, M. I. Wilson, R. Bicknell, K.-U. Eckardt, P. H. Maxwell, P. J. Ratcliffe, and C. W. Pugh, 2002. Peptide blockade of HIFα degradation modulates cellular metabolism and angiogenesis. *Proc. Natl. Acad. Sci.* 99(16):10423–10428.

[14] Chen, Y.-N. P., S. K. Sharma, T. M. Ramsey, L. Jiang, M. S. Martin, K. Baker, P. D. Adams, K. W. Bair, and W. G. Kaelin Jr., 1999. Selective killing of transformed cells by cyclin/cyclin-dependent kinase 2 antagonists. *Proc. Natl. Acad. Sci. USA* 96(8):4325–4329.

[15] Mendoza, N., S. Fong, J. Marsters, H. Koeppen, R. Schwall, and D. Wickramasinghe, 2003. Selective Cyclin-dependent Kinase 2/Cyclin A Antagonists that Differ from ATP Site Inhibitors Block Tumor Growth. *Cancer Res.* 63(5):1020–1024.

[16] Harbour, J. W., L. Worley, D. Ma, and M. Cohen, 2002. Transducible peptide therapy for uveal melanoma and retinoblastoma. *Arch. Ophthalmol.* 120(10):1341–1346.

[17] Mai, J. C., Z. Mi, S.-H. Kim, B. Ng, and P. D. Robbins, 2001. A Proapoptotic Peptide for the Treatment of Solid Tumors. *Cancer Res.* 61 (21):7709–7712.

[18] Datta, K., C. Sundberg, S. A. Karumanchi, and D. Mukhopadhyay, 2001. The 104–123 Amino Acid Sequence of the β-domain of von Hippel-Lindau Gene Product Is Sufficient to Inhibit Renal Tumor Growth and Invasion. *Cancer Res.* 61 (5):1768–1775.

[19] Hosotani, R., Y. Miyamoto, K. Fujimoto, R. Doi, A. Otaka, N. Fujii, and M. Imamura, 2002. Trojan p16 Peptide Suppresses Pancreatic Cancer Growth and Prolongs Survival in Mice. *Clin. Cancer Res.* 8(4):1271–1276.

[20] Zhou, J., J. Fan, and J.-T. Hsieh, 2006. Inhibition of Mitogen-Elicited Signal Transduction and Growth in Prostate Cancer with a Small Peptide Derived from the Functional Domain of DOC-2/DAB2 Delivered by a Unique Vehicle. *Cancer Res.* 66(18):8954–8958.

[21] Snyder, E., B. Meade, C. Saenz, and S. Dowdy, 2004. Treatment of Terminal Peritoneal Carcinomatosis by a Transducible p53-Activating Peptide. *PLoS Biology* 2(2):0186–0193.

[22] Haase, H., G. Dobbernack, G. Tünnemann, P. Karczewski, M. C. Cardoso, D. Petzhold, W. P. Schlegel, S. Lutter, P. Pierschalek, J. Behlke, and I. Morano, 2006. Minigenes encoding N-terminal domains of human cardiac myosin light chain-1 improve heart function of transgenic rats. *FASEB J* 20 (7):865–873.

[23] Tünnemann, G., P. Karczewski, H. Haase, M. C. Cardoso, and I. Morano, 2007. Modulation of muscle contraction by a cell-permeable peptide. *J Mol Med* 85(12):1405–1412.

[24] Cahill, K. E., 2009. Simple model of the transduction of cell-penetrating peptides. *IET Syst. Biol.* 3(5):300–306.

[25] Cahill, K. E., 2010. Cell-penetrating peptides, electroporation and drug delivery. *IET Syst. Biol.* 4(6):367–378.

[26] Herce, H. D., A. E. Garcia, J. Litt, R. S. Kane, P. Martin, N. Enrique, A. Rebolledo, and V. Milesi, 2009. Arginine-Rich Peptides Destabilize the Plasma Membrane, Consistent with a Pore Formation Translocation Mechanism of Cell-Penetrating Peptides. *Biophys. J.* 97(7):1917–1925.

[27] Bai, J., and E. R. Chapman, 2004. The C2 domains of synaptotagmin—partners in exocytosis. *TRENDS Biochem. Sci.* 29(3):143–151.

[28] Ralf Mohrmann, R., H. de Wit, M. Verhage, E. Neher, and J. B. Srensen, 2010. Fast Vesicle Fusion in Living Cells Requires at Least Three SNARE Complexes. *Science* 330:502–505.

[29] Korobkova, E., T. Emonet, J. Vilar, T. Shimizu, and P. Cluzel, 2004. From molecular noise to behavioral variability in a single bacterium. *Nature* 428:574–578.

[30] Emonet, T. Signaling noise coordinates multiple flagella to enhance bacterial foraging with minimal cost to chemotactic response. Talk at qbio4 in 2010.

[31] Cahill, K. Fortran 90 codes for this paper. `http://bio.phys.unm.edu/lipidBilayer`.